AIP | APL Materials

New strain states and radical property tuning of metal oxides using a nanocomposite thin film approach

Judith MacManus-Driscoll, Ady Suwardi, Ahmed Kursumovic, Zhenxing Bi, Chen-Fong Tsai, Haiyan Wang, Quanxi Jia, and Oon Jew Lee

Citation: APL Mater. **3**, 062507 (2015); doi: 10.1063/1.4919059
View online: http://dx.doi.org/10.1063/1.4919059
View Table of Contents: http://scitation.aip.org/content/aip/journal/aplmater/3/6?ver=pdfcov
Published by the AIP Publishing

APL MATERIALS **3**, 062507 (2015)

New strain states and radical property tuning of metal oxides using a nanocomposite thin film approach

Judith MacManus-Driscoll,[1,a] Ady Suwardi,[1] Ahmed Kursumovic,[1] Zhenxing Bi,[2] Chen-Fong Tsai,[3] Haiyan Wang,[2,3] Quanxi Jia,[4] and Oon Jew Lee[1,b]

[1]*Device Materials Group, Department of Materials Science and Metallurgy, University of Cambridge, Cambridge CB3 0FS, United Kingdom*
[2]*Department of Electrical and Computer Engineering, Texas A&M University, College Station, Texas 77843, USA*
[3]*Material Science and Engineering Program, Texas A&M University, College Station, Texas 77843, USA*
[4]*Center for Integrated Nanotechnologies (CINT), Los Alamos National Laboratory, Los Alamos, New Mexico 87545, USA*

(Received 6 March 2015; accepted 15 April 2015; published online 5 May 2015)

Auxetic-like strain states were generated in self-assembled nanocomposite thin films of $(Ba_{0.6}Sr_{0.4}TiO_3)_{1-x} - (Sm_2O_3)_x$(BSTO – SmO). A switch from auxetic-like to elastic-like strain behavior was observed for $x > 0.50$, when the SmO switched from being nanopillars in the BSTO matrix to being the matrix with BSTO nanopillars embedded in it. A simple model was adopted to explain how *in-plane* strain varies with x. At high x (0.75), strongly enhanced ferroelectric properties were obtained compared to pure BSTO films. The nanocomposite method represents a powerful new way to tune the properties of a wide range of strongly correlated metal oxides whose properties are very sensitive to strain. [http://dx.doi.org/10.1063/1.4919059]

Vertical heteropitaxial nanocomposite thin films are proving to be increasingly important for creating advanced multifunctional oxide thin films with new properties.[1] In these composites, new phenomena also occur giving a very powerful way to tune device functionality. Very high ferroelectric Curie temperatures,[2] strongly improved dielectric tunability,[3] reducing dielectric loss,[4] enhanced multiferroic coupling,[5] photostriction-magnetic coupling,[6] strongly enhanced current densities in superconductors,[7] new kinds of memristor devices,[8] and strongly enhanced ionic conduction at lower temperatures have all been reported.[9,10]

However, the understanding and origin of unusual strain states in nanocomposite films have not been explored to date. On the other hand, strain is critical to tuning the properties of strongly correlated metal oxide films where bond lengths and angles strongly influence the wide-ranging functional phenomena. What is known is that compared to planar thin films, the strain in vertical nanocomposites does not relax when the film grows thicker. This is due to the fact that vertical lattice epitaxy between the phases dominates the strain state of the system, making the substrate contribution *insignificant* above a few 10's of nm where the strain relaxes.[11] What is not known is how and why auxetic-like strain effects arise in nanocomposite films. In a previous study, we showed auxetic-like strain in nanocomposite microactuator films of $(BaTiO_3)_{0.5}$ $(Sm_2O_3)_{0.5}$. The transverse piezoelectric coefficient, d_{31}, in the films was positive instead of negative as observed in the standard thin film case. Also, at room temperature, the magnitude of d_{31} at >200 pm V^{-1} exceeded PZT films.[12] In a similar system of $(Ba_{0.6}Sr_{0.4}TiO_3)_{0.25}(Sm_2O_3)_{0.75}$, we showed that both tunability and

[a]Author to whom correspondence should be addressed. Electronic mail: jld35@cam.ac.uk
[b]This research was performed while Oon Jew Lee was at Device Materials Group, Department of Materials Science and Metallurgy, University of Cambridge, Cambridge CB3 0FS, United Kingdom.

dielectric loss could be simultaneously improved which is the opposite case for standard composites of $Ba_{0.6}Sr_{0.4}TiO_3$. Again, unusual strain states were thought to be responsible.[3]

In this work, we explore the strain states in the $(Ba_{0.6}Sr_{0.4}TiO_3)_{1-x}$ $(Sm_2O_3)_x$ $((BSTO)_x - (SmO)_{1-x})$ thin film system. The system is ideal from the chemical point of view because there is minimal intermixing between the two component phases.[8] A simple model which incorporates thermal expansion mismatch and lattice mismatch strain between the phases was used to understand how and why the *in-plane* and *out-of-plane* lattice parameters vary with x in the way they do. Finally, the ferroelectric properties of the films were probed and the enhanced properties observed explained in terms of the strain states observed.

Nanocomposite thin films were fabricated from 5 different ceramic targets of $((BSTO)_x - (SmO)_{1-x})$ with x = 0.00, 0.25, 0.50, 0.75, and 1.00. The targets were made by mixing and grinding $Ba_{0.6}Sr_{0.4}TiO_3$ and Sm_2O_3 powders together followed by sintering at 1300 °C overnight. The $Ba_{0.6}Sr_{0.4}TiO_3$ powder was synthesized by mixing 99.99% pure $BaTiO_3$ and $SrTiO_3$ with 99.99% Sm_2O_3 powder. Pulsed laser deposition (PLD) using a KrF excimer laser with 1 Hz repetition rate, a laser fluence of ~2 J/cm^2, and an oxygen pressure of 20 Pa was used to grow the films. The films were grown onto (001) single crystal $SrTiO_3$ (STO) substrates with 30 nm thick buffer layers of $SrRuO_3$ (SRO). The SRO layers were first deposited off-axis at 700 °C and then the BSTO-SmO deposited at 800 °C. No special growth measures had to be taken to make the films self-assemble into a structure composed of "vertical nanopillars of one phase in a matrix of the other phase" with a high level of epitaxy. BSTO-SmO film thicknesses of 300 nm, 600 nm, and 1000 nm were explored.

High resolution X-ray diffraction (XRD), transmission electron microscopy (TEM), and scanning electron microscopy (SEM) were used to obtain crystallographic and microstructural information on the films. Atomic force microscopy (AFM) in piezoforce mode and polarization versus electric field (P-E) hysteresis loops were measured to determine the ferroelectric properties of the films.

For x = 0.25 and 0.50, the BSTO forms the matrix and the SmO forms the columns, whereas for x = 0.75, the SmO forms the matrix and the BSTO forms the columns.[3] TEM images of $(BSTO)_{1-x} - (SmO)_x$ films comparing lower and higher x values, where the BSTO either forms the matrix (x = 0.50) or the columns (x = 0.75), are shown in Figs. 1(a) and 1(b), respectively. Fig. 1(c) is a sketch of the microstructure of the x = 0.25 and 0.50 films. The column diameters are ~10 nm with 10-80 nm spacing, depending on x. The SEM plan view image in the inset of Fig. 1(c) clearly reveals the vertically aligned nano-columns embedded in a film matrix. As shown in an earlier paper,[3] the epitaxial relationship of the BSTO and SmO phases on the SRO/STO substrate is (002)BSTO||(004)SmO||(002)SRO||(002)STO and (020)BSTO||(220)SmO||(020)SRO||(020)STO. The (220) direction of SmO phase is parallel to the (020) of the STO substrate phase, because the unit cell of SmO grows 45° rotated relative to the STO unit cell. This rotation is energetically

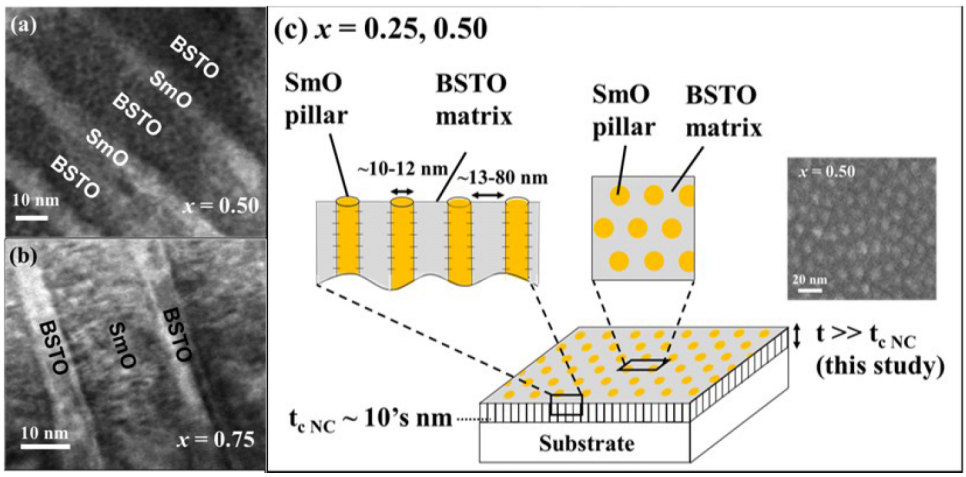

FIG. 1. Microstructures of $(BSTO)_{1-x} - (SmO)_x$ nanocomposite films for different x values. Transmission electron micrographs for (a) x = 0.50, (b) x = 0.75. (c) Schematic diagram showing nanocomposite structure for x = 0.25, 0.50, and plan view SEM image of surface of x = 0.50 film revealing nanopillars.

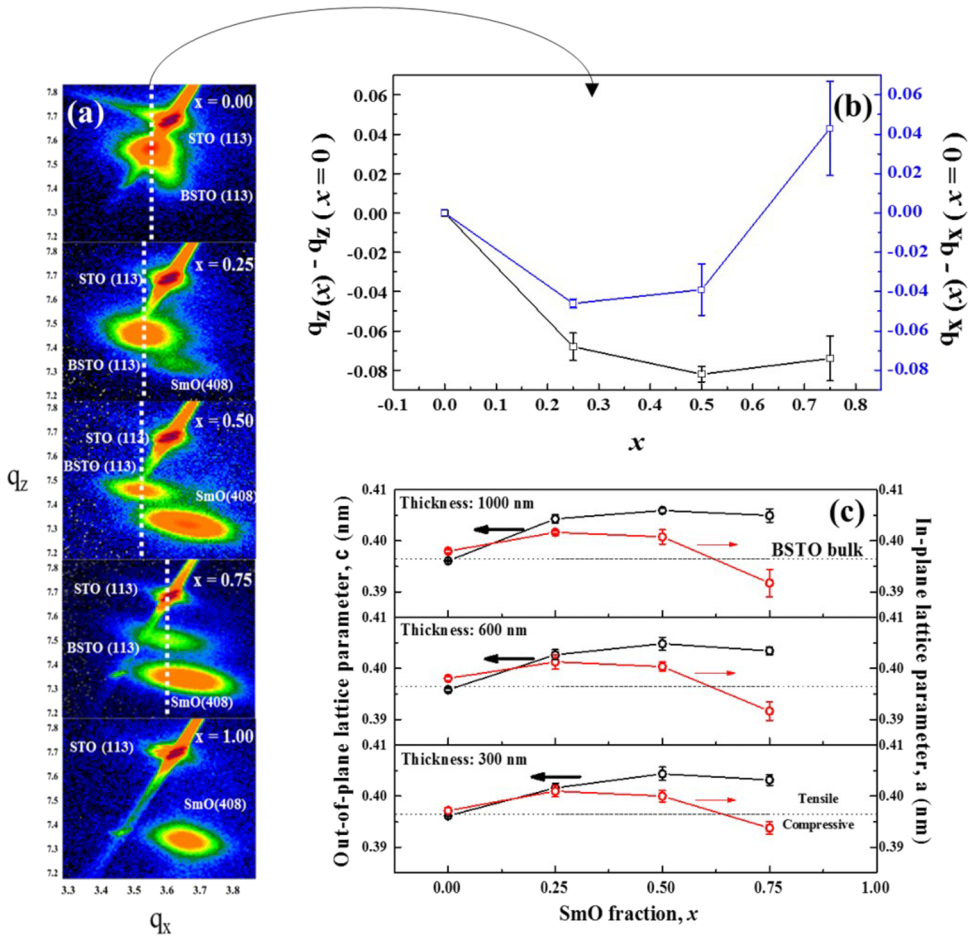

FIG. 2. (a) Reciprocal space maps of $(BSTO)_{1-x}-(SmO)_x$ nanocomposite films, near the (113) perovskite peaks, with compositions ranging from pure BSTO ($x = 0.00$) to pure SmO ($x = 1.00$). (b) *In-plane* and *out-of-plane* shift of the (113) BSTO peak positions for different x values with respect to $x = 0.00$. (c) *Out-of-plane* and *in-plane* lattice parameters of BSTO for various thicknesses versus x.

favorable as it enables SmO lattice matching of $1.0927/4 \times \sqrt{2} = 0.3863$ nm with [100] (0.3905 nm) in STO.[11]

The lattice parameters of the films were determined from a combination of XRD reciprocal space maps (RSMs) of the asymmetric (113) reflections and $2\theta - \omega$ scans (not shown) of the symmetric (00l) peaks (Figs. 2(a) and 2(b)). The analysis assumes that the BSTO is tetragonal which is expected from the literature.[3]

Concentrating first on the RSMs and *in-plane* parameters, we focus on the position of the BSTO (113) peaks along q_x. The position of the centers of these peaks along q_x is shown by the white dashed lines and they indicate how the *in-plane* a lattice parameters change with x (Fig. 2(b)). At $x = 0.00$, a broad BSTO (113) peak is observed and it is shifted to the left compared to the STO (113) peak, indicative of a fully relaxed film, and an *in-plane* lattice parameter of BSTO which is larger than STO. The relaxation is expected for a film of this large thickness. As x increases from 0.00 to 0.25, the (113) peaks are shifted markedly to the left indicating a strong tensile strain *in-plane*. The peak is also sharpened. Together these findings indicate that there is progressively increased strain control of the BSTO by the SmO phase with increasing x. For $x = 0.50$, the peak remains in approximately the same position in q_x as at $x = 0.25$ but is sharpened much further indicative of full strain control of BSTO by the SmO phase. This is consistent with the BSTO lateral spacing between the pillars decreasing from ~80 nm to ~10-15 nm, thereby allowing for full vertical epitaxial strain control in the BSTO, i.e., insufficient lateral thickness to allow for stress relaxation.

On going from $x = 0.50$ to $x = 0.75$, the BSTO (113) peak position shifts strongly to the right, being at a similar position to the STO substrate peak. At this large x value, the SmO film forms the matrix with the BSTO forming the nanocolumns of ~10 nm size in the SmO (Fig. 1(c)). The BSTO rods are under compressive strain *in-plane* which represents a complete switch from the tensile strain found when the BSTO is the matrix for $x = 0.25$ and 0.50.

The *out-of-plane c* lattice parameters of the BSTO phase were obtained from the 2θ - ω scans (not shown). There was a clear increase in c with x. This trend is observed also from downward shift of the (113) BSTO peak centers in the RSMs with increasing x. The *in-plane a* lattice parameters were calculated based on the (113) peak positions in the RSM scans. Both a and c lattice parameters are plotted as a function of x and thickness (300 nm-1000 nm) in Fig. 2(c). The bulk cubic BSTO lattice parameter is also included for comparison.

Across the entire thickness range, the pure BSTO ($x = 0.00$) films are fully relaxed, as confirmed by their lattice parameter values being the same as the bulk values for BSTO. This result is expected since at 300 nm and above, the films are no longer under epitaxial strain control by the substrate, i.e., all the films are well above the critical thickness and are relaxed. On the other hand, for all x values >0.00 and for all thicknesses, the c axis is larger than the bulk value, and hence, the BSTO is always in tension *out-of-plane*. The *out-of-plane* expansion results from vertical strain control of the BSTO (elastic modulus ~80 GPa) by the stiffer SmO (elastic modulus ~220 GPa).[13,14]

Looking now at the *in-plane* lattice parameters of BSTO, as already discussed qualitatively for the RSMs of Fig. 2(a), we see that with increasing x, the *in-plane* parameters of the BSTO increase rapidly upon introduction of a moderate fraction ($x = 0.25$) of SmO into the films, but then stay approximately the same from $x = 0.25$ to $x = 0.50$. For both these x values, the SmO phase is in the form of strain-controlling nanopillars in the BSTO matrix. Since both a and c are expanded for these compositions, the films are exhibiting an auxetic-like behavior. The tensile strain in both directions is high, depending on x and film thickness, and is as high as 2.4% for $x = 0.50$ and 1000 nm thickness. Indeed, the vertical strain state is highest in the thickest films, which is opposite to the case of plain films. This is a unique feature of nanocomposite films.[2] At $x = 0.75$, the *in-plane* parameter decreases markedly and now the BSTO appears to show a normal elastic-like behavior. As already mentioned, at this x value, the BSTO forms fine nanopillars (~10 nm) embedded within a SmO matrix, the lateral thickness of SmO between the pillars being ~40 nm (Fig. 1(b)).

For $x = 0.25$ and $x = 0.50$, in order to understand the observed unusual auxetic effect in the films we employ a simple model to calculate the BSTO lattice parameters: to determine the c parameter, we consider the vertical lattice parameter control of the BSTO phase by the SmO, and to determine the a parameter, we consider the *in-plane* thermal shrinkage of the film upon cooling after growth.

First we consider the ***out-of-plane*** strain in the BSTO. We first note that the influence of the substrate on the ***out-of-plane*** strain in the nanocomposite case is negligible. This is because the film thicknesses studied here (>300 nm) are all above the critical thickness for the nanocomposite, tc_{NC}, which is a few 10's of nm thickness,[11] as shown in Fig. 1(c). tc_{NC} depends on the vertical column/matrix area relative to the substrate/film area. Above tc_{NC}, the vertical column/matrix area exceeds the substrate/film area and then the substrate does not determine the strain state of the film. Instead, the stiffer phase in the composite determines the strain state of the softer phase in the composite. We note that the critical thickness for standard planar films (or superlattices), tc_{PL}, above which the film strain is relaxed and is no longer fixed by epitaxy control from the substrate, is much larger than for nanocomposite films. The value of tc_{PL} is ~100 nm.[1,15]

The *out-of-plane* strain in the BSTO is dominated by vertical epitaxy between it and the SmO, no matter whether the x value is high or low: the BSTO phase is strained by the much stiffer SmO pillars. Domain matching epitaxy (DME) determines how many lattices of the respective phases match with one another and this controls the overall strain level.[11] From Fig. 2(c), it is observed that for all film thicknesses, the *out-of-plane* lattice parameter increases with x. This is explained by the lateral size of the BSTO decreasing with increasing x, which means the SmO can exert a greater influence on the BSTO with less strain relaxation taking place. We do not calculate the variation of the *out-of-plane* lattice parameter with x as it is not easy to predict the extent of strain relaxation with x.

In planar multilayers, the substrate controls the *in-plane* lattice parameters with the *out-of-plane* lattice parameters controlled by the resulting elastic deformation in accordance with Poisson effect. For the nanocomposite films, a very different situation occurs. At above tc_{NC} (i.e. at all the film thicknesses of this study), as previously mentioned, the substrate does not play a role in setting the lattice parameters.

Next, we consider the ***in-plane*** strain in the BSTO. Upon cooling, from the growth temperature, the BSTO thermal shrinkage is very close to STO, and hence, the room temperature BSTO lattice parameters will not be influenced by the substrate. This is confirmed by the $x = 0.00$ lattice parameters being the same as the bulk values (Fig. 3(a)). It is important next to consider the influence of the SmO nanopillars on the *in-plane* straining of BSTO. The soft BSTO matrix is "epitaxially anchored" everywhere by the dense, stiff, scaffold SmO pillars of spacing ~80 nm ($x = 0.25$) and ~10-15 nm ($x = 0.50$), embedded in the matrix. Hence, the BSTO and SmO are "glued," together with the stiffer SmO controlling the behaviour of the softer BSTO. Hence, because

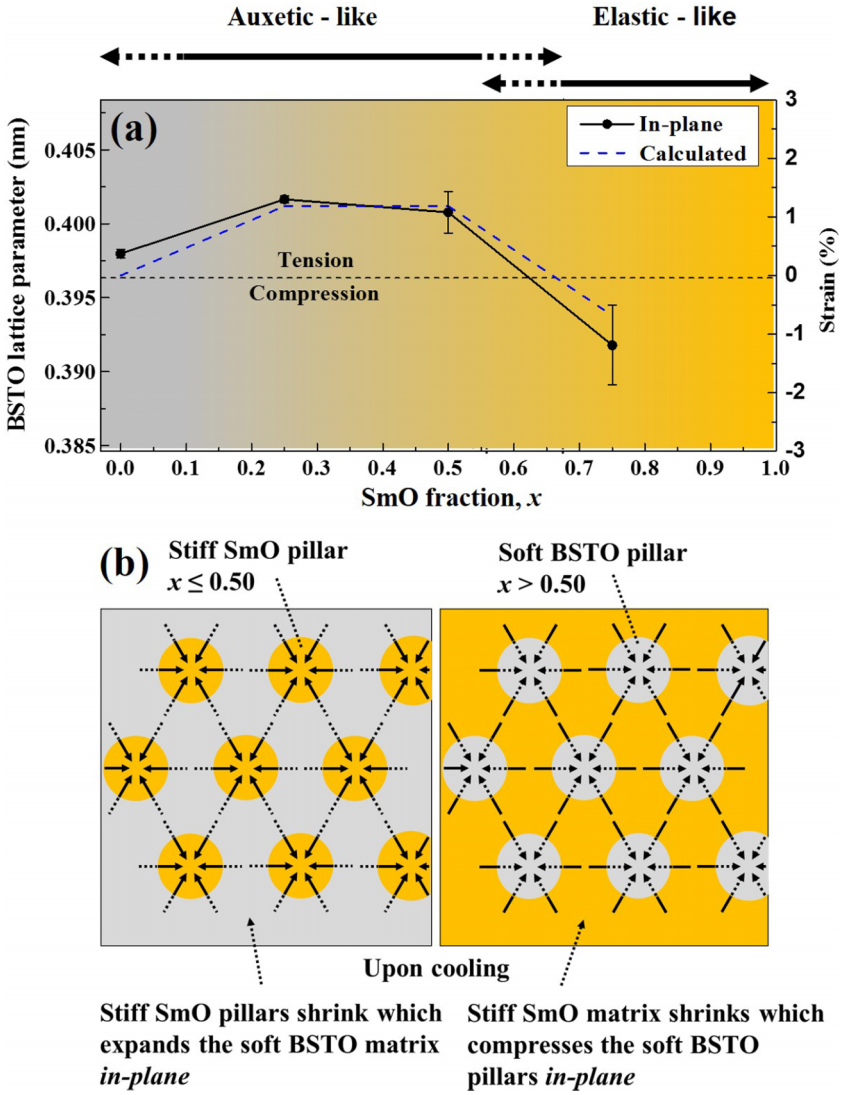

FIG. 3. (a) Experimental and modelled values of BSTO *in-plane* lattice parameter (left hand axis) and corresponding *in-plane* strain (right hand axis) versus x for the 1000 nm thickness nanocomposite films. (b) Schematic diagram showing the SmO thermal shrinkage effect on the *in-plane* BSTO strain upon cooling films from the growth temperature. Low x (left image) and high x (right image).

of the anchoring effect, it is not appropriate to consider a weighted averaging (depending on x) of the thermal expansion coefficients of each phase.

The pillars' contraction is not limited to or by the substrate contraction since the area that each pillar has with the substrate is minimal compared to their length which is significantly above tc_{NC}. Hence, upon cooling from the growth temperature, the SmO pillars can contract freely. The epitaxial anchoring of the BSTO to the SmO will mean that BSTO is prevented from contracting (as shown schematically in Fig. 3(b)). Thus, there is an *in-plane* expansion of the BSTO lattice of exactly opposite magnitude to the contraction of the SmO,

$$\varepsilon\|\text{BSTO} = -\varepsilon\|\text{SmO}, \text{where } \varepsilon\|\text{SmO} = \alpha_{\text{SmO}}\Delta T,$$

where $\varepsilon\|$BSTO is the *in-plane* strain in the BSTO phase, $\varepsilon\|$SmO is the *in-plane* strain in the SmO, and α_{SmO} is the coefficient of thermal expansion of the SmO phase which is 8.8×10^{-6} K^{-1} Ref. 16 and ΔT is taken to be −775 K, i.e., the difference between the growth temperature and room temperature.

Hence, $\varepsilon\|\text{BSTO} = 8.8 \times 10^{-6}\,K^{-1} \times 775 = 0.68\%$.

Furthermore, the expansion of the BSTO by the SmO (both *in-plane* and *out-of-plane*) will prevent the cubic to tetragonal phase transformation in BSTO from taking place which would normally occur near room temperature for BSTO of this composition.[17] The absence of a phase transformation leads to an additional *in-plane* lattice parameter expansion of ∼0.50%, i.e., the opposite sign of the normal contraction of the *in-plane* lattice parameters upon cooling through T_C.[18] We note that for x values between 0.00 and 0.25, the distance between SmO nanopillars will become too large to allow the anchoring to be effective at all places in the BSTO matrix. Hence, at places far away from the SmO pillars, the BSTO will be relaxed and the auxetic-like effect will then not occur.

The above two calculated *in-plane* expansions of the BSTO, i.e. (1) the thermal contraction of the SmO, and (2) the prevention of the cubic to tetragonal phase transition, giving (1+2), the total *in-plane* expansion of the BSTO, are given in Table I, together with the sum of these two expansions, and the measured values. The calculated and measured *in-plane* lattice parameters (for the 1000 nm film) are also shown in Fig. 3(a). The calculated total *in-plane* strain values compare favorably to the measured values.

We note that in the *out-of-plane* direction, upon cooling there will also be some contraction of the BSTO lattice owing to the SmO contraction and the higher stiffness SmO forcing the BSTO to follow it, just as for the *in-plane* case. Overall, however, the c-axis lattice parameter will still be expanded considerably from the DME vertical epitaxy strain.

For $x = 0.75$, the BSTO now forms the nanocolumns (of ∼10 nm diameter) and the SmO forms the matrix (Fig. 1(b)). In all the film thicknesses, the SmO has its fully relaxed bulk lattice parameter, i.e., 1.0927 nm. This bulk lattice parameter is expected since although the film is a composite, it will not have any additional strain influence from the BSTO pillars since they are softer than the

TABLE I. Calculated and experimental values of the *in-plane* strain and BSTO lattice parameters in $(BSTO)_{1-x}(SmO)_x$ nanocomposite thin films. The calculation for $x = 0.25$ and 0.50 case differs to the $x = 0.75$ case. While in both cases the thermal contraction of the stiff SmO dominates the *in-plane* BSTO lattice parameters, in the case of $x = 0.25$ and 0.50 the SmO was in the form of pillars in a BSTO matrix, and hence upon cooling the pillars tense the BSTO matrix. On the other hand, for $x = 0.75$ the SmO forms the matrix and it compresses the embedded BSTO pillars. STO lattice parameters $a = b = c = 0.3905$ nm (JCPDS 35-0734), BSTO lattice parameters $a = b = c = 0.3965$ nm (JCPDS 34-0411), SmO lattice parameters $a = b = c = 1.0927$ nm (JCPDS 15-0813).

x	(1) Thermal expansion strain $\varepsilon_{\|\text{BSTO}}$ $(-\alpha_{\text{SmO}}\Delta T)$ (%)	(2) FE phase transition strain $(c/a = 1.01)$ (%)	(1+2) Total Calculated *in-plane* strain (%)	Measured *in-plane* strain (%)	Calculated BSTO *in-plane* lattice parameter (nm)	Measured BSTO *in-plane* lattice parameter (nm)
0.25	0.68	0.50	1.18	1.31 ± 0.07	0.4012	0.4017 ± 0.0003
0.50	0.68	0.50	1.18	1.08 ± 0.35	0.4012	0.4008 ± 0.0014
0.75	−0.68	N/A	−0.68	−1.19 ± 0.68	0.3938	0.3918 ± 0.0027

matrix. Also, the films have thickness above tc_{PL}, and so, full strain relaxation is expected. This is very different to the mirror situation of the $x = 0.25$ composition where BSTO is the matrix and does not relax to the bulk lattice parameter because the stiff SmO pillars control the behavior of the matrix, as discussed above.

The *in-plane* strain in the BSTO nanopillars will be equivalent to the thermal shrinkage strain from the enveloping, stiffer SmO matrix which radially squeezes the pillars upon cooling of the film after growth (see schematic diagram in Fig. 3(b)). Here, since the BSTO matrix is not under tension *in-plane*, the cubic to tetragonal phase transition is not prevented from occurring as in the $x = 0.25$ and 0.50 cases. The overall BSTO compression is therefore just $\varepsilon\|\text{BSTO} = \varepsilon\|\text{SmO} = \alpha_{\text{SmO}}\Delta T = -0.68\%$. The value is consistent with the measured parameter as shown in Table I.

Finally, the intrinsic polarization of the BSTO-SmO films is discussed. Fig. 4(a) shows the P-E hysteresis loops of the 300 nm thick BSTO-SmO films compared to pure BSTO and SmO films of similar thickness. The saturation polarization, *Psat*, of the BSTO-SmO nanocomposite films (taken at 300 kV/cm and normalized by the area of BSTO in each film) increases monotonically with an increase of x in the order, $Psat$, $x = 0.75 >> Psat$, $x = 0.50 >> Psat$, $x = 0.25 >> Psat$ $x = 0$. As expected, the pure SmO films are not ferroelectric (inset to Fig. 4(a)) and hence do not contribute to the ferroelectric polarization of the BSTO-SmO nanocomposite films. The $Psat$, $x = 0$ (pure BSTO) value is similar to the literature for similar-composition BSTO films.[17] The $Psat$, $x = 0.75$

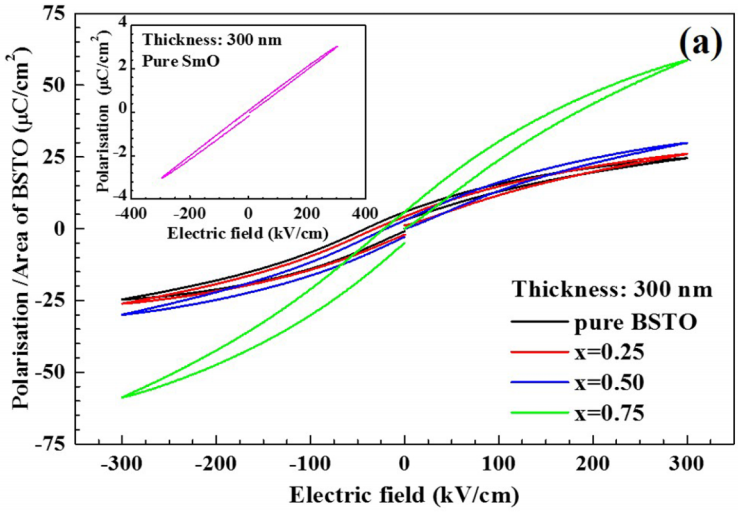

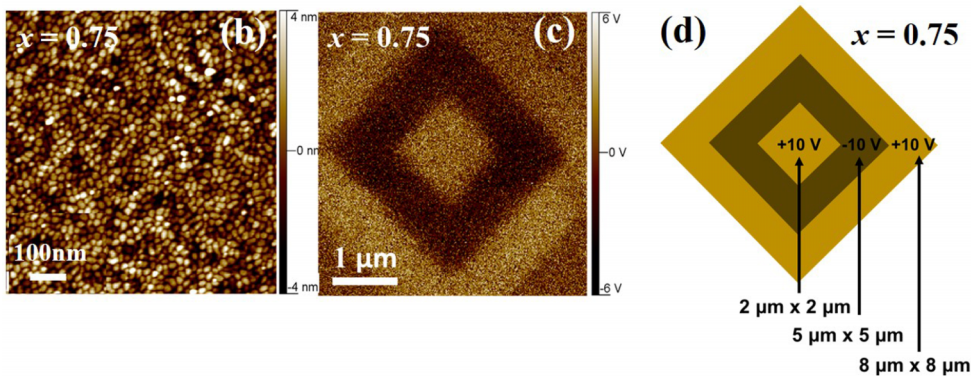

FIG. 4. (a) Polarization versus electric field hysteresis loops for $(BSTO)_{1-x}-(SmO)_x$ films for different x values. Pure SmO film ($x = 1$) shown in the inset. (b) AFM topography image of $x = 0.75$ film with 1 μm × 1 μm scan area, (c) piezoresponse phase image of $x = 0.75$ film with multiple polings with different scan areas, and (d) schematic of the multiple poling areas with an applied DC bias of ±10 V.

value is much higher than BSTO or BTO films from the literature by almost 300%.[19] In composite films, the effective dielectric constant of the films is a function of surface area of two different phases or the composition. This is expected if we consider the dielectric constant of the composite as two capacitors (with different dielectric constants) connected in parallel. For instance, the nominal dielectric constant for the pure BSTO film (~300 nm) is about 1080 at frequency from 10 kHz to 1 MHz. The measured dielectric constant of the composite film ($x = 0.75$) with the same film thickness is around 400. The calculated dielectric constant of the composite for this specific composition is less than 280 if we assume a dielectric constant of 1080 for the pure BSTO film. The much larger effective dielectric constant of the composite films implies that the dielectric constant of BSTO phase is much enhanced due to the lattice strain in the composite films.

Since the *out-of-plane* lattice strain is similar for $x = 0.50$ and $x = 0.75$ but since *Psat*, $x = 0.75$ is much larger for $x = 0.75$, it is clear the magnitude of *Psat*, does not depend on the *out-of-plane* tension alone. We recall that for $x = 0.75$, we have clean, highly tetragonally distorted, ~10 nm nanopillars, whereas at $x = 0.50$, we have an auxetic-like strained BSTO matrix with a high density of SmO nanopillars penetrating it. The nanoscale nature of the BSTO, combined with the large *in-plane* compression, are clearly important additional factors for enhancing *Psat*.

Piezo-response force microscopy (PFM) measurements with multiple polings confirm the strong ferroelectric nature of the BSTO-SmO, $x = 0.75$ films. The *out-of-plane* piezo-response phase contrast images (shown in Fig. 4(c)) are observed with multiple switching when an AC modulating voltage of ±5 V and DC bias of ±10 V (Fig. 4(d)) were applied to the SRO bottom electrode at an excitation frequency of 10 kHz. In comparison to a topography image with a 1 μm × 1 μm scan area, the influence of microstructure on piezo-switching effect is minor (Fig. 4(b)). The 45° rotated dark and bright regions with various scan areas of 8 μm × 8 μm, 5 μm × 5 μm, and 2 μm × 2 μm show the domain reorientations corresponding to −10 V and +10 V. This observation supports the strong ferroelectric polarization measured in the P-E loops (Fig. 4(a)).

In summary, strain states in up to 1000 nm thick heteroepitaxial nanocomposite thin films of $(Ba_{0.6}Sr_{0.4}TiO_3)_{1-x} - (Sm_2O_3)_x$ (BSTO-SmO) on $SrTiO_3$ were studied. Unusual auxetic-like tensile strain was observed for $x = 0.25$ and $x = 0.50$, whereas elastic-like strain was observed for $x = 0.75$. The *in-plane* strain and lattice parameters of BSTO were modeled by considering the influence that the stiff SmO has on the softer BSTO upon cooling the films from the growth temperature. Very good agreement was found between calculation and experiment. For $x = 0.25$ and 0.50, the BSTO matrix is expanded *in-plane* as a result of the thermal shrinkage of the stiff SmO nanopillars which are epitaxially anchored to the BSTO matrix and hence control its expansion/contraction. The expansion of the BSTO has the additional effect of preventing the cubic to tetragonal phase transition in the BSTO from occurring. Overall, the BSTO lattice is expanded both *in-plane* and *out-of-plane*, the *out-of-plane* lattice parameter being determined by vertical heteroepitaxial straining of the BSTO by the SmO. For $x = 0.75$, the SmO forms the matrix and the BSTO forms the pillars, and it acts to "squeeze" the nanopillars *in-plane*. Hence, for $x = 0.75$, the BSTO shrinks *in-plane*, while it is still expanded *out-of-plane* as before. Owing to this high *out-of-plane* tension and *in-plane* compression, the BSTO shows a very high *Psat*, $x = 0.75$ value of ~120 $\mu C/cm^2$ for a 1000 nm film thickness, much higher than standard plain BSTO or BTO films.

More globally, we have demonstrated a very simple way to create unusual auxetic-like strain states in strongly correlated thin film metal oxides, thus allowing for radically new and different physical properties to be engineered into them.

This work was supported by the European Research Council (ERC) (Advanced Investigator Grant No. ERC-2009-AdG-247276-NOVOX). A. Suwardi acknowledges support from the Agency of Science, Technology and Research (A*STAR), Singapore. The work at Texas A&M was funded by the U.S. National Science Foundation (Nos. DMR-1401266 and DMR-0846504). The work at Los Alamos was partially supported by the Laboratory Directed Research and Development Program and was performed, in part, at the Center for Integrated Nanotechnologies, an Office of Science User Facility operated for the U.S. Department of Energy (DOE) Office of Science.

[1] J. L. MacManus-Driscoll, Adv. Funct. Mater. **20**(13), 2035 (2010).
[2] S. A. Harrington, J. Zhai, S. Denev, V. Gopalan, H. Wang, Z. Bi, S. A. T. Redfern, S.-H. Baek, C. W. Bark, and C.-B. Eom, Nat. Nanotechnol. **6**(8), 491 (2011).

[3] O. J. Lee, S. A. Harrington, A. Kursumovic, E. Defay, H. Wang, Z. Bi, C.-F. Tsai, L. Yan, Q. Jia, and J. L. MacManus-Driscoll, Nano Lett. **12**(8), 4311 (2012).
[4] H. Yang, H. Wang, G. F. Zou, M. Jain, N. A. Suvorova, D. M. Feldmann, P. C. Dowden, R. F. DePaula, J. L. MacManus-Driscoll, and A. J. Taylor, Appl. Phys. Lett. **93**(14), 142904 (2008).
[5] T. Fix, E.-M. Choi, J. W. A. Robinson, S. B. Lee, A. Chen, B. Prasad, H. Wang, M. G. Blamire, and J. L. MacManus-Driscoll, Nano Lett. **13**(12), 5886 (2013).
[6] H.-J. Liu, L.-Y. Chen, Q. He, C.-W. Liang, Y.-Z. Chen, Y.-S. Chien, Y.-H. Hsieh, S.-J. Lin, E. Arenholz, and C.-W. Luo, ACS Nano **6**(8), 6952 (2012).
[7] S. A. Harrington, J. H. Durrell, B. Maiorov, H. Wang, S. C. Wimbush, A. Kursumovic, J. H. Lee, and J. L. MacManus-Driscoll, Supercond. Sci. Technol. **22**(2), 022001 (2009).
[8] S. Lee, A. Sangle, P. Lu, A. Chen, W. Zhang, J. S. Lee, H. Wang, Q. Jia, and J. L. MacManus-Driscoll, Adv. Mater. **26**(36), 6284 (2014).
[9] Q. Su, D. Yoon, A. Chen, F. Khatkhatay, A. Manthiram, and H. Wang, J. Power Sources **242**, 455 (2013).
[10] V. T. Tra, J.-C. Yang, Y.-H. Hsieh, J.-Y. Lin, Y.-C. Chen, and Y.-H. Chu, Phys. Status Solidi RRL **8**(6), 478 (2014).
[11] J. L. MacManus-Driscoll, P. Zerrer, H. Wang, H. Yang, J. Yoon, A. Fouchet, R. Yu, M. G. Blamire, and Q. Jia, Nat. Mater. **7**(4), 314 (2008).
[12] A. Kursumovic, E. Defay, O. J. Lee, C.-F. Tsai, Z. Bi, H. Wang, and J. L. MacManus-Driscoll, Adv. Funct. Mater. **23**(47), 5881 (2013).
[13] T.-H. Fang, W.-J. Chang, C.-M. Lin, L.-W. Ji, Y.-S. Chang, and Y.-J. Hsiao, Mater. Sci. Eng.: A **426**(1), 157 (2006).
[14] D. S. D. Gunn, N. L. Allan, and J. A. Purton, J. Mater. Chem. A **2**(33), 13407 (2014).
[15] S. C. Wimbush, M. Li, M. E. Vickers, B. Maiorov, D. Matt Feldmann, Q. Jia, and J. L. MacManus-Driscoll, Adv. Funct. Mater. **19**(6), 835 (2009).
[16] S. Stecura and W. J. Campbell, *Thermal Expansion and Phase Inversion of Rare-Earth oxides* (US Department of the Interior, Bureau of Mines, 1961).
[17] Z.-G. Ban and S. P. Alpay, J. Appl. Phys. **91**(11), 9288 (2002).
[18] S. Banerjee and P. Mukhopadhyay, *Phase Transformations: Examples from Titanium and Zirconium Alloys* (Elsevier, 2010).
[19] B. Jaffe, *Piezoelectric Ceramics* (Elsevier, 2012).